The Astrophysical Journal Letters, 953:L28 (10pp), 2023 August 20 https://doi.org/10.3847/2041-8213/acec3e

IXPE and Multiwavelength Observations of Blazar PG 1553+113 Reveal an Orphan Optical Polarization Swing

Riccardo Middei[1,2], Matteo Perri[1,2], Simonetta Puccetti[1], Ioannis Liodakis[3], Laura Di Gesu[4], Alan P. Marscher[5], Nicole Rodriguez Cavero[6], Fabrizio Tavecchio[7], Immacolata Donnarumma[4], Marco Laurenti[8,9], Svetlana G. Jorstad[5,10], Iván Agudo[11], Herman L. Marshall[12], Luigi Pacciani[13], Dawoon E. Kim[13,14,15], Francisco José Aceituno[11], Giacomo Bonnoli[7,11], Víctor Casanova[11], Beatriz Agís-González[11], Alfredo Sota[11], Carolina Casadio[16,17], Juan Escudero[11], Ioannis Myserlis[18,19], Albrecht Sievers[18], Pouya M. Kouch[3,20], Elina Lindfors[3], Mark Gurwell[21], Garrett K. Keating[21], Ramprasad Rao[21], Sincheol Kang[22], Sang-Sung Lee[22,23], Sang-Hyun Kim[22,23], Whee Yeon Cheong[22,23], Hyeon-Woo Jeong[22,23], Emmanouil Angelakis[24], Alexander Kraus[19], Lucio A. Antonelli[1,25], Matteo Bachetti[26], Luca Baldini[27,28], Wayne H. Baumgartner[29], Ronaldo Bellazzini[27], Stefano Bianchi[30], Stephen D. Bongiorno[29], Raffaella Bonino[31,32], Alessandro Brez[27], Niccolò Bucciantini[33,34,35], Fiamma Capitanio[13], Simone Castellano[27], Elisabetta Cavazzuti[36], Chien-Ting Chen[37], Stefano Ciprini[1,38], Enrico Costa[13], Alessandra De Rosa[13], Ettore Del Monte[13], Niccolò Di Lalla[39], Alessandro Di Marco[13], Victor Doroshenko[40], Michal Dovčiak[41], Steven R. Ehlert[29], Teruaki Enoto[42], Yuri Evangelista[13], Sergio Fabiani[13], Riccardo Ferrazzoli[13], Javier A. García[43], Shuichi Gunji[44], Kiyoshi Hayashida[45,66], Jeremy Heyl[46], Wataru Iwakiri[47], Philip Kaaret[29], Vladimir Karas[41], Fabian Kislat[48], Takao Kitaguchi[42], Jeffery J. Kolodziejczak[29], Henric Krawczynski[49], Fabio La Monaca[13], Luca Latronico[31], Simone Maldera[31], Alberto Manfreda[50], Frédéric Marin[51], Andrea Marinucci[36], Francesco Massaro[31,32], Giorgio Matt[30], Ikuyuki Mitsuishi[52], Tsunefumi Mizuno[53], Fabio Muleri[13], Michela Negro[54,55,56], Chi-Yung Ng[57], Stephen L. O'Dell[29], Nicola Omodei[39], Chiara Oppedisano[31], Alessandro Papitto[25], George G. Pavlov[58], Abel L. Peirson[39], Melissa Pesce-Rollins[27], Pierre-Olivier Petrucci[59], Maura Pilia[26], Andrea Possenti[26], Juri Poutanen[20], Brian D. Ramsey[29], John Rankin[13], Ajay Ratheesh[13], Oliver J. Roberts[37], Roger W. Romani[39], Carmelo Sgrò[27], Patrick Slane[60], Paolo Soffitta[13], Gloria Spandre[27], Douglas A. Swartz[37], Toru Tamagawa[42], Roberto Taverna[61], Yuzuru Tawara[52], Allyn F. Tennant[29], Nicholas E. Thomas[29], Francesco Tombesi[15,38,62], Alessio Trois[26], Sergey S. Tsygankov[20], Roberto Turolla[61,63], Jacco Vink[64], Martin C. Weisskopf[29], Kinwah Wu[63], Fei Xie[13,65], and Silvia Zane[63]

[1] Space Science Data Center, Agenzia Spaziale Italiana, Via del Politecnico snc, I-00133 Roma, Italy; riccardo.middei@ssdc.asi.it
[2] INAF Osservatorio Astronomico di Roma, Via Frascati 33, I-00078 Monte Porzio Catone (RM), Italy
[3] Finnish Centre for Astronomy with ESO, University of Turku, FI-20014 Turky, Finland
[4] ASI—Agenzia Spaziale Italiana, Via del Politecnico snc, I-00133 Roma, Italy
[5] Institute for Astrophysical Research, Boston University, 725 Commonwealth Avenue, Boston, MA 02215, USA
[6] Physics Department, McDonnell Center for the Space Sciences, and Center for Quantum Leaps, Washington University in St. Louis, St. Louis, MO 63130, USA
[7] INAF Osservatorio Astronomico di Brera, Via E. Bianchi 46, I-23807 Merate (LC), Italy
[8] INFN—Sezione di Roma "Tor Vergata," Via della Ricerca Scientifica 1, I-00133 Roma, Italy
[9] Space Science Data Center, SSDC, ASI, Via del Politecnico snc, I-00133 Roma, Italy
[10] Saint Petersburg State University, 7/9 Universitetskaya nab., St. Petersburg 199034 Russia
[11] Instituto de Astrofísica de Andalucía, IAA-CSIC, Glorieta de la Astronomía s/n, E-18008 Granada, Spain
[12] MIT Kavli Institute for Astrophysics and Space Research, Massachusetts Institute of Technology, 77 Massachusetts Avenue, Cambridge, MA 02139, USA
[13] INAF Istituto di Astrofisica e Planetologia Spaziali, Via del Fosso del Cavaliere 100, I-00133 Roma, Italy
[14] Dipartimento di Fisica, Università degli Studi di Roma "La Sapienza," Piazzale Aldo Moro 5, I-00185 Roma, Italy
[15] Dipartimento di Fisica, Università degli Studi di Roma "Tor Vergata," Via della Ricerca Scientifica 1, I-00133 Roma, Italy
[16] Institute of Astrophysics, Foundation for Research and Technology—Hellas, Voutes, 7110 Heraklion, Greece
[17] Department of Physics, University of Crete, 70013 Heraklion, Greece
[18] Institut de Radioastronomie Millimétrique, Avenida Divina Pastora, 7, Local 20, E-18012 Granada, Spain
[19] Max-Planck-Institut für Radioastronomie, Auf dem Hügel 69, D-53121 Bonn, Germany
[20] Department of Physics and Astronomy, University of Turku, FI-20014 Turku, Finland
[21] Center for Astrophysics | Harvard & Smithsonian, 60 Garden Street, Cambridge, MA 02138 USA
[22] Korea Astronomy and Space Science Institute, 776 Daedeok-daero, Yuseong-gu, Daejeon 34055, Republic of Korea
[23] University of Science and Technology, Korea, 217 Gajeong-ro, Yuseong-gu, Daejeon 34113, Republic of Korea
[24] Section of Astrophysics, Astronomy & Mechanics, Department of Physics, National and Kapodistrian University of Athens, Panepistimiopolis Zografos 15784, Greece
[25] INAF Osservatorio Astronomico di Roma, Via Frascati 33, I-00040 Monte Porzio Catone (RM), Italy
[26] INAF Osservatorio Astronomico di Cagliari, Via della Scienza 5, I-09047 Selargius (CA), Italy
[27] Istituto Nazionale di Fisica Nucleare, Sezione di Pisa, Largo B. Pontecorvo 3, I-56127 Pisa, Italy
[28] Dipartimento di Fisica, Università di Pisa, Largo B. Pontecorvo 3, I-56127 Pisa, Italy
[29] NASA Marshall Space Flight Center, Huntsville, AL 35812, USA
[30] Dipartimento di Matematica e Fisica, Università degli Studi Roma Tre, Via della Vasca Navale 84, I-00146 Roma, Italy
[31] Istituto Nazionale di Fisica Nucleare, Sezione di Torino, Via Pietro Giuria 1, I-10125 Torino, Italy
[32] Dipartimento di Fisica, Università degli Studi di Torino, Via Pietro Giuria 1, I-10125 Torino, Italy
[33] INAF Osservatorio Astrofisico di Arcetri, Largo Enrico Fermi 5, I-50125 Firenze, Italy
[34] Dipartimento di Fisica e Astronomia, Università degli Studi di Firenze, Via Sansone 1, I-50019 Sesto Fiorentino (FI), Italy
[35] Istituto Nazionale di Fisica Nucleare, Sezione di Firenze, Via Sansone 1, I-50019 Sesto Fiorentino (FI), Italy
[36] Agenzia Spaziale Italiana, Via del Politecnico snc, I-00133 Roma, Italy
[37] Science and Technology Institute, Universities Space Research Association, Huntsville, AL 35805, USA
[38] Istituto Nazionale di Fisica Nucleare, Sezione di Roma "Tor Vergata", Via della Ricerca Scientifica 1, I-00133 Roma, Italy

[39] Department of Physics and Kavli Institute for Particle Astrophysics and Cosmology, Stanford University, Stanford, CA 94305, USA
[40] Institut für Astronomie und Astrophysik, Universität Tübingen, Sand 1, D-72076 Tübingen, Germany
[41] Astronomical Institute of the Czech Academy of Sciences, Boční II 1401/1, 14100 Praha 4, Czech Republic
[42] RIKEN Cluster for Pioneering Research, 2-1 Hirosawa, Wako, Saitama 351-0198, Japan
[43] California Institute of Technology, Pasadena, CA 91125, USA
[44] Yamagata University, 1-4-12 Kojirakawa-machi, Yamagata-shi 990-8560, Japan
[45] Osaka University, 1-1 Yamadaoka, Suita, Osaka 565-0871, Japan
[46] University of British Columbia, Vancouver, BC V6T 1Z4, Canada
[47] International Center for Hadron Astrophysics, Chiba University, Chiba 263-8522, Japan
[48] Department of Physics and Astronomy and Space Science Center, University of New Hampshire, Durham, NH 03824, USA
[49] Physics Department and McDonnell Center for the Space Sciences, Washington University in St. Louis, St. Louis, MO 63130, USA
[50] Istituto Nazionale di Fisica Nucleare, Sezione di Napoli, Strada Comunale Cinthia, I-80126 Napoli, Italy
[51] Université de Strasbourg, CNRS, Observatoire Astronomique de Strasbourg, UMR 7550, F-67000 Strasbourg, France
[52] Graduate School of Science, Division of Particle and Astrophysical Science, Nagoya University, Furo-cho, Chikusa-ku, Nagoya, Aichi 464-8602, Japan
[53] Hiroshima Astrophysical Science Center, Hiroshima University, 1-3-1 Kagamiyama, Higashi-Hiroshima, Hiroshima 739-8526, Japan
[54] University of Maryland, Baltimore County, Baltimore, MD 21250, USA
[55] NASA Goddard Space Flight Center, Greenbelt, MD 20771, USA
[56] Center for Research and Exploration in Space Science and Technology, NASA/GSFC, Greenbelt, MD 20771, USA
[57] Department of Physics, University of Hong Kong, Pokfulam, Hong Kong
[58] Department of Astronomy and Astrophysics, Pennsylvania State University, University Park, PA 16801, USA
[59] Université Grenoble Alpes, CNRS, IPAG, F-38000 Grenoble, France
[60] Center for Astrophysics, Harvard & Smithsonian, 60 Garden St, Cambridge, MA 02138, USA
[61] Dipartimento di Fisica e Astronomia, Università degli Studi di Padova, Via Marzolo 8, I-35131 Padova, Italy
[62] Department of Astronomy, University of Maryland, College Park, MD 20742, USA
[63] Mullard Space Science Laboratory, University College London, Holmbury St Mary, Dorking, Surrey RH5 6NT, UK
[64] Anton Pannekoek Institute for Astronomy & GRAPPA, University of Amsterdam, Science Park 904, 1098 XH Amsterdam, The Netherlands
[65] Guangxi Key Laboratory for Relativistic Astrophysics, School of Physical Science and Technology, Guangxi University, Nanning 530004, People's Republic of China

Received 2023 June 23; revised 2023 July 26; accepted 2023 July 30; published 2023 August 22

Abstract

The lower-energy peak of the spectral energy distribution of blazars has commonly been ascribed to synchrotron radiation from relativistic particles in the jets. Despite the consensus regarding jet emission processes, the particle acceleration mechanism is still debated. Here, we present the first X-ray polarization observations of PG 1553 +113, a high-synchrotron-peak blazar observed by the Imaging X-ray Polarimetry Explorer (IXPE). We detect an X-ray polarization degree of $(10 \pm 2)\%$ along an electric-vector position angle of $\psi_X = 86° \pm 8°$. At the same time, the radio and optical polarization degrees are lower by a factor of $\sim$3. During our IXPE pointing, we observed the first orphan optical polarization swing of the IXPE era, as the optical angle of PG 1553+113 underwent a smooth monotonic rotation by about 125°, with a rate of $\sim 17°$ day^{-1}. We do not find evidence of a similar rotation in either radio or X-rays, which suggests that the X-ray and optically emitting regions are separate or, at most, partially cospatial. Our spectropolarimetric results provide further evidence that the steady-state X-ray emission in blazars originates in a shock-accelerated and energy-stratified electron population.

Unified Astronomy Thesaurus concepts: BL Lacertae objects (158); Spectropolarimetry (1973); Polarimetry (1278); Active galactic nuclei (16); Jets (870); X-ray active galactic nuclei (2035)

1. Introduction

Blazars, a rare class of active galactic nuclei (AGNs; Antonucci 1993; Urry & Padovani 1995; Padovani et al. 2017), display highly time-variable radiation across the entire electromagnetic spectrum, from radio to very-high-energy (TeV) γ-rays (e.g., Angel & Stockman 1980; Padovani & Giommi 1995; Fossati et al. 1998; Ghisellini et al. 1998; Sreekumar et al. 1998; Abdo et al. 2010; Maselli et al. 2010; Agudo et al. 2011a, 2011b; Acero et al. 2015; Liodakis et al. 2018b, 2019; Hovatta & Lindfors 2019). It is widely accepted that the nonthermal radiation originates in a highly collimated jet of relativistic particles extended along the polar axis of an accreting supermassive black hole (SMBH) and pointing toward the Earth (see, e.g., Blandford et al. 2019). Despite accretion of matter onto the SMBHs powering blazars, their orientation is such that highly relativistically boosted radiation from the jet dominates the emission spectrum (e.g., Lähteenmäki & Valtaoja 1999; Hovatta et al. 2009; Liodakis et al. 2018a), with a double-peaked spectral energy distribution (SED). The first hump peaks between infrared (IR) and X-ray frequencies, and is ascribed to synchrotron radiation from energetic electrons, perhaps, as suggested by previous Imaging X-ray Polarimetry Explorer (IXPE) pointings, accelerated in shocks (e.g., Di Gesu et al. 2022; Liodakis et al. 2022). The second hump is located in the GeV–TeV range, with the mechanism behind the emission still debated. Both hadronic and leptonic frameworks have been proposed (e.g., Maraschi et al. 1992; Boettcher 2012; Cerruti et al. 2015), although recent X-ray spectropolarimetric observations seem to favor a leptonic scenario in which synchrotron self-Compton emission plays a key role in shaping the SED of some blazars (see, e.g., Middei et al. 2023; Peirson et al. 2023). Depending on the frequency at which the synchrotron component peaks ($\nu_{\rm peak}$), blazars are classified as high synchrotron peak (HSP), intermediate synchrotron peak (ISP), or low synchrotron peak

[66] Deceased.

Table 1
Log of the IXPE and XMM-Newton Observations of PG 1553+113

Observatory	Obs. ID	Obs. Date yyyy-mm-dd/dd	Net Exp. (ks)
IXPE(a)	02004999	2023-02-1/3	∼98
IXPE(b)	02004999	2023-02-8/9	∼28
XMM-Newton	0902112101	2023-01-31	∼14

(LSP,) with $\nu_{\rm peak} > 10^{15}$ Hz, $10^{14} < \nu_{\rm peak} < 10^{15}$ Hz, and $\nu_{\rm peak} < 10^{14}$ Hz, respectively (e.g., Ajello et al. 2020).

PG 1553+113 (R.A. $= 15^{\rm h}55^{\rm m}43\overset{\rm s}{.}0440$, decl. $= +11°11'24\overset{''}{.}365$, J2000) is an HSP source ($\nu_{\rm peak} \approx 3.9 \times 10^{15}$ Hz; Ajello et al. 2020); therefore, X-rays sample the falling part of the low-energy hump of its SED. Although several redshift values ($z < 0.5$) have been reported for this BL Lacertae object, the most commonly adopted value is $z = 0.433$ (see, e.g., Nicastro et al. 2018; Johnson et al. 2019; Dorigo Jones et al. 2022). It is a TeV γ-ray emitter (Aleksić et al. 2012), and has exhibited one of the most compelling cases of quasi-periodic oscillations from a blazar at γ-ray energies as a period $p = 2.18 \pm 0.08$ yr was found in the γ-rays (Ackermann et al. 2015; Tavani et al. 2018).

Here we present the first X-ray polarization observation of PG 1553+113, an HSP blazar observed by the IXPE (Weisskopf et al. 2022) in 2023 February. Owing to the three gas pixel detectors (GPDs; Costa et al. 2001; Bellazzini et al. 2003; Baldini et al. 2021) in its focal plane, IXPE provides an unprecedented opportunity to measure the X-ray polarization of cosmic sources. Since its launch on 2021 December 9, IXPE has observed different types of AGNs (e.g., Ehlert et al. 2022; Marinucci et al. 2022; Gianolli et al. 2023; Ingram et al. 2023; Tagliacozzo et al. 2023; Ursini et al. 2023), including blazars (e.g., Di Gesu et al. 2022; Liodakis et al. 2022; Middei et al. 2023). PG 1553+113 is one of several HSP blazars observed by IXPE. In Section 2 we report on the data reduction, while Section 3 discusses the X-ray emission and polarization properties of PG 1553+113. In Section 4 we present the contemporaneous radio and optical polarization observations, and in Section 5 we summarize and discuss our results and draw conclusions.

2. X-Ray Data Reduction

PG 1553+113 was observed with IXPE's three detector units (DUs) in 2023 February for a total exposure time of ∼130 ks. The observing time was split into two intervals (hereafter, intervals a and b). Interval a was taken on 2023 February 1–2, for a total net exposure time of ∼100 ks. Interval b, performed one week later on February 8–9, had a net exposure time of ∼30 ks.

We coordinated the IXPE observations with XMM-Newton (Jansen et al. 2001) and the Neil Gehrels Swift Observatory (Swift; Gehrels et al. 2004), which observed the target before and after the IXPE observation. Table 1 reports the log for the IXPE and XMM-Newton pointings.

We extracted the I, Q, and U spectra for each of the three DUs of IXPE using the software IXPEOBSSIM (v.30.0.0; Pesce-Rollins et al. 2019; Baldini et al. 2022) and following the background rejection prescriptions presented in Di Marco et al. (2023). Moreover, spectra were computed in order to use the so-called weighted analysis method presented in Di Marco et al. (2022; parameter STOKES = NEFF in XSELECT). The spectra for the Stokes parameters were computed from a circular region with radius $= 0\overset{'}{.}95$ centered on the source, while an annulus with $r_{\rm in(out)} = 1\overset{'}{.}2(3\overset{'}{.}5)$ was adopted to extract the background. This approach has been shown to enhance the sensitivity to polarization (Di Marco et al. 2023). The resulting I Stokes spectra were grouped by requiring each energy bin to have a signal-to-noise ratio (S/N) greater than 7. We adopted uniform binning of 280 eV for the Q and U Stokes spectra.

XMM-Newton performed a snapshot (∼14 ks long) of PG 1553+113, and we analyzed the data taken with the EPIC-pn camera (Strüder et al. 2001). The source was observed in Small Window mode, with the medium filter applied. We processed the data via the standard XMM-Newton Science Analysis System (SAS v21; Gabriel et al. 2004). Source extraction radii and screening for high-background intervals were determined through an iterative process (Piconcelli et al. 2004) that maximizes the S/N. The background was extracted from circular regions with a radius of 50″, and the same shape centered on the source PG 1553+113 was adopted for science products. The resulting third-level products were grouped by requiring each bin to contain at least 30 counts, and not to oversample the spectral resolution by a factor larger than 3. The net count rate was less than the maximum allowed limit of 50 counts s^{-1} to avoid deteriorated response due to photon pileup for EPIC-pn observations in Small Window mode (e.g., Jethwa et al. 2015). We further assessed the potential impact of pileup in the XMM-Newton observation by means of the *epatplot* task, a standard SAS command devoted to checking for any pileup affecting the data, and we found it to be negligible.

Swift pointed at PG 1553+113 before and after the IXPE pointing. Sixteen exposures, each 1 ks long, were taken in photon counting mode and calibrated and reduced using the *XRTDAS* software package.[67] To extract the source spectra, we adopted a circular region of radius 47″, while the background was derived with a concentric annulus with inner (outer) radii of 120″ (150″). Spectra were then binned, with at least 25 counts in each bin, in order to use the χ^2 statistic meaningfully in our spectral analysis.

3. X-Ray Analysis

The X-ray spectropolarimetric analysis was performed using XSPEC (Arnaud 1996) and following the prescriptions of the so-called weighted analysis method (Di Marco et al. 2022). We accounted for Galactic absorption along the line of sight using the `tbabs` model. In all the fits, we set the Galactic column density to $n_{\rm H} = 3.62 \times 10^{20}$ cm^{-2} (HI4PI Collaboration et al. 2016). For calculations involved the distance to PG 1553+113, we adopt the standard cosmological framework with $H_0 = 70$ km s^{-1} Mpc^{-1} and $\Lambda_0 = 0.73$.

3.1. IXPE and XMM-Newton Spectropolarimetric Analysis

To determine the spectral properties of PG 1553+113, we modeled the 0.3–10 keV XMM-Newton spectrum (taken contemporaneously with the IXPE observation; see Table 1). We tested two models: an absorbed power law and an absorbed logarithmic parabola. The log-parabola (Massaro et al. 2004) is defined by $N(E) = (E/E_1)^{-\alpha-\beta\log(E/E_1)}$, where α accounts for the source photon index at energy E_1, β represents the

[67] https://sda2006.ts.infn.it/presentazioni/capalbi.pdf

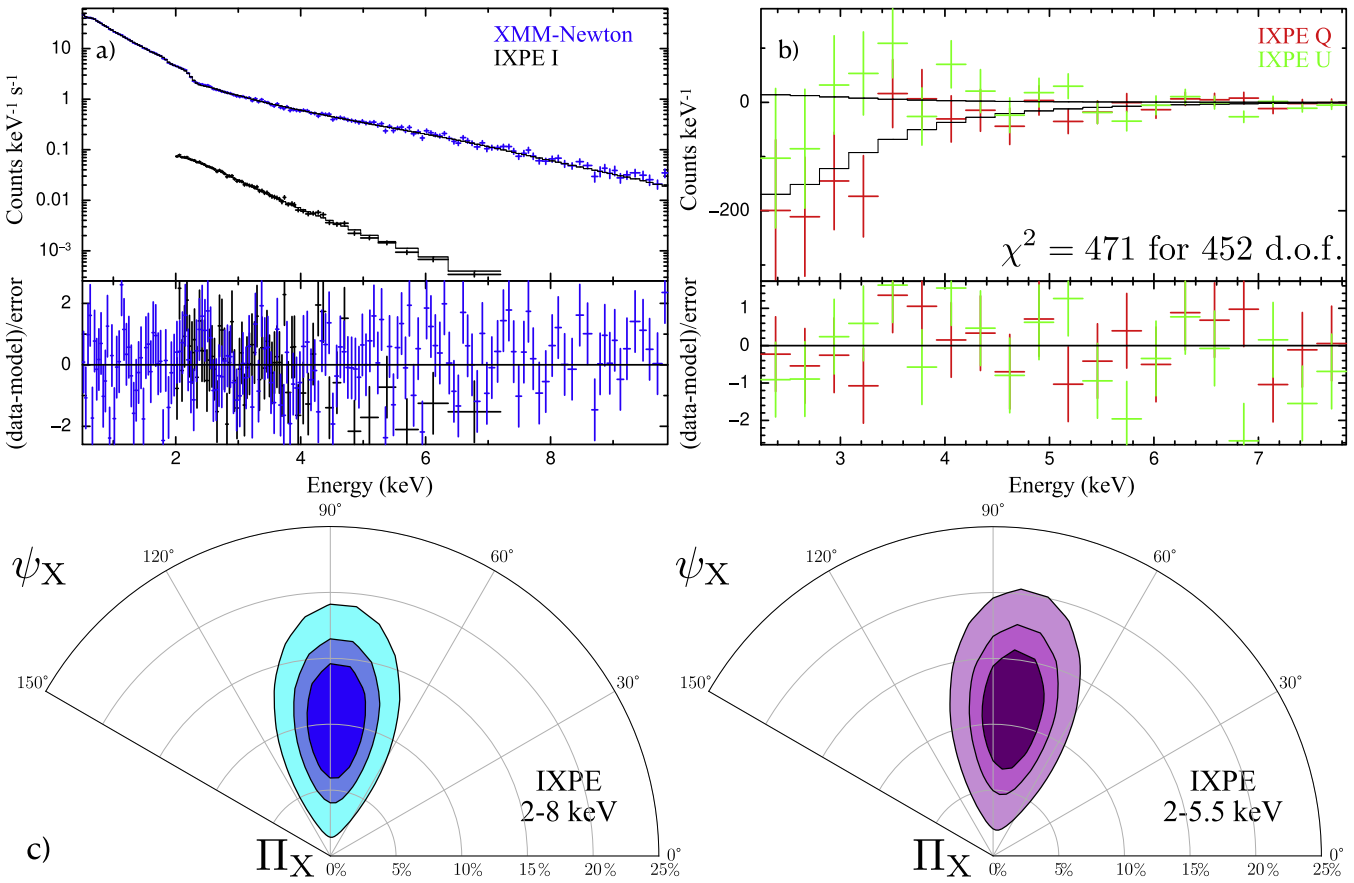

Figure 1. Top panels: best fit to the IXPE and XMM-Newton data and corresponding residuals. On the left, we show the model `const×polconst×logpar` fitting the *I* Stokes spectra, while on the right the best-fit *Q* and *U* Stokes spectra are shown. Bottom panels: regions accounting for 68%, 90%, and 99% confidence levels computed using the full IXPE 2–8 keV data (bottom left) or taking into account the IXPE *I*, *Q*, and *U* Stokes spectra only in the 2–5.5 keV range.

curvature of the parabola, and E_1 is a reference ("pivot") energy. In the fits, we determined the photon index and normalization for the power law. For the log-parabola, we fixed E_1 to 3 keV and left α, β, and the normalization free to vary. The power law fails to reproduce the XMM-Newton spectrum satisfactorily ($\chi^2/\mathrm{dof} = 530/159$), while the logarithmic parabola returns a better statistic, with $\chi^2 = 219$ for 159 degrees of freedom (dof). We obtained $\alpha = 2.50 \pm 0.01$ and $\beta = 0.13 \pm 0.01$, which are compatible with a soft and curved spectrum, as expected for a blazar X-ray spectrum dominated by synchrotron radiation. We note that this fit can be further improved ($\Delta\chi^2 = -41$ for two additional dof) by adding a narrow Gaussian component to account for an additional soft X-ray feature ($E = 0.68$ keV and Norm $= 2.58 \times 10^{-4}$ photons cm^{-2} s^{-1}). Finally, we notice that IXPE caught PG 1553+113 in a fairly high flux state compared with the average flux of this source ($F_{\mathrm{mean}} \sim 2.1 \times 10^{-11}$ erg cm^{-2} s^{-1} in the 2–10 keV energy range) obtained by Giommi et al. (2021) who analyzed 802 Swift archival snapshots of the blazar.

Next, we included in the analysis the IXPE spectra extracted from both the a and b intervals. We assigned each spectrum to a "data group" in XSPEC, which allowed us to couple/decouple the parameters of the model between the different instruments when needed. As a first test, we assumed the polarization properties of PG 1553+113 to be the same in the two observing intervals. Thus, we fit the corresponding *I*, *Q*, and *U* Stokes spectra while constraining the relevant parameters. To account for polarization, we updated our XSPEC model to `tbabs×const×polconst×logpar`. The constant model (`const`) allows for cross-calibration among the different IXPE DUs and the EPIC-pn camera. The polarization model `polconst`, which assumes constant polarization parameters within the operating energy range, has two free parameters: the polarization degree (Π_X) and the electric-vector position angle (Ψ_X, measured from north through east). Finally, for the `logpar` model, we coupled the α and β parameters between the IXPE and XMM-Newton spectra. This model provided a statistically acceptable ($\chi^2/\mathrm{dof} = 471/452$) fit to the IXPE and XMM-Newton data, which is shown in Figure 1 (panels (a) and (b) for the *I* and *Q* and *U* Stokes parameters, respectively). The corresponding best-fit parameters are listed in Table 2. Our fit result suggests that the spectrum of PG 1553+113 had a soft and curved shape ($\alpha = 2.49 \pm 0.01$ and $\beta = 0.11 \pm 0.01$). These values are well within the range of what is commonly observed for HSP blazars (e.g., Middei et al. 2022). The polarization properties were determined to be $\Pi_X = (10.1 \pm 2.3)\%$ and $\psi_X = 86° \pm 8°$. In Figure 1(c) we show the contours corresponding to 68%, 90%, and 99% confidence levels. We find the polarized signal to be a maximum in terms of significance in the 2–5.5 keV energy range. The soft and curved shape of the spectrum, and the maximum polarization signal measured below 5.5 keV, are in agreement with the PG 1553+113 X-ray spectrum being dominated by synchrotron emission. We also search for a possible dependence of the polarization degree and angle on the energy. However, the present data set is compatible with a constant Π_X and ψ_X, see

Table 2
Best-fit Parameters from the Spectropolarimetric Analysis of PG 1553+113

Model	Parameter	Time Average	Interval a	Interval b
polconst	Π_X	$(10.1 \pm 2.3)\%$	$(11.6 \pm 3.4)\%$	$<26\%$
	ψ_X	$86° \pm 8°$	$85° \pm 8°$	⋯
tbabs	n_H	3.62†	3.62†	3.62 †
log-par	α	2.491 ± 0.007	2.59 ± 0.03	2.56 ± 0.15
	β	0.11 ± 0.01	0.11†	0.11†
	Norm	1.49 ± 0.02	1.41 ± 0.03	1.43 ± 0.02
const	K_{Du2}	0.91 ± 0.01	0.95 ± 0.01	0.96 ± 0.07
const	K_{Du3}	0.95 ± 0.01	0.90 ± 0.01	0.97 ± 0.07
const	$K_{Epic\text{-}pn}$	1.04 ± 0.01	⋯	⋯
$F_{2-8\ keV}$		2.55 ± 0.03	2.47 ± 0.03	2.44 ± 0.05

Note. The "time average" results refer to the IXPE and XMM-Newton joint fit, while values quoted for intervals a and b were obtained only with the IXPE data. Fluxes are in units of 10^{-11} erg cm^{-2} s^{-1} while the logarithmic parabola has a normalization of 10^{-3}. All errors are given for the 68% confidence interval for one parameter of interest (i.e., $\Delta\chi^2 = 1$), while the upper limit to the polarization degree corresponds to 99% uncertainty. The symbol † indicates those parameters that were kept frozen during the model fits.

Table 2, when computing these quantities for different energy bins (2–3, 2–3.5, 2–4, 2–5, 2–5.5, 2–6, and 2–7 keV).

We further investigated for a possible change in the polarization properties of PG 1553+113 between observation intervals a and b. Using the model `tbabs×const×polconst×logpar`, we computed α, the normalization, Π_X, and ψ_X from the Stokes parameters derived for intervals a and b separately. In this test the curvature parameter β was kept frozen to its best-fit value indicated in Table 2.[68] The adoption of the `tbabs×const×polconst×logpar` model led us to a very good representation of the two data sets, with $\chi^2/\mathrm{dof} = 304/276$ and $\chi^2/\mathrm{dof} = 285/276$ for intervals a and b, respectively. The inferred best-fit parameters are listed in Table 2. Despite the compatible 2–8 keV flux observed in the two intervals, Π_X and ψ_X are only constrained within interval a, while an upper limit $\Pi_X^{99\%} < 26\%$ is obtained when fitting the Stokes I, Q, and U spectra from interval b. This upper limit is likely the result of the relatively short duration of the b interval exposure. As a final test, we studied the polarization properties of PG 1553+113 over time spans shorter than the durations of intervals a and b of the IXPE observation. However, for all the tested temporal intervals no hints of variability were found.

3.2. Swift Monitoring Campaign

A Swift campaign was organized to monitor the flux and spectral variability of PG 1553+113. The XRT observed the blazar from 2023 early January until late February. We fit the resulting 16 spectra (exposures of $\leqslant$1 ks each) with a log-parabola model, with Galactic absorption (see above). The adopted model provides a statistically acceptable representation of the data. We show the spectral parameters and flux estimates inferred from the fits in Figure 2. The Swift data are compatible with nearly constant spectral shape and variability of flux by less than a factor of 2. The average values for the quantities displayed in Figure 2 are $\alpha_{avg} = 2.15 \pm 0.12$ and $\beta_{avg} = 0.3 \pm 0.2$, with fluxes $F_{IXPE}^{avg} = 3.4 \pm 0.6$ (2–8 keV), $F_{Soft}^{avg} = 4.6 \pm 0.5$ (0.5–2 keV), and $F_{Hard}^{avg} = 3.7 \pm 0.6$ (2–10 keV) in units of 10^{-11} erg cm^{-2} s^{-1}.

[68] For this test we did not considered the XMM-Newton data, as they were taken just before the IXPE interval a exposure.

4. Multiwavelength Observations

PG 1553+113 was also observed at radio and optical wavelengths by the Effelsberg 100 m telescope, the Korean VLBI Network (KVN), Institut de Radioastronomie Millimétrique (IRAM) 30 m telescope, Submillimeter Array (SMA), Boston University Perkins Telescope, Calar Alto Observatory, Nordic Optical Telescope, and the Sierra Nevada Observatory. The observational and data analysis procedures are described in detail in Middei et al. (2023). All the multiwavelength observations are available upon request to the individual observatories. We supplement our campaign with 3 day binned publicly available Fermi Large Area Telescope data from the light curve repository[69] (Abdollahi et al. 2023).

At radio wavelengths, the Effelsberg observation on 2023 February 8 (MJD 59983.14) was performed at 4.85 GHz as part of the Monitoring the Stokes Q, U, I, and V Emission of AGN jets in Radio (QUIVER) program (Kraus et al. 2003; Myserlis et al. 2018). The IRAM 30 m observations were obtained and analyzed in the framework of the Polarimetric Monitoring of AGN at Millimeter Wavelengths (POLAMI) project[70] (Agudo et al. 2018a, 2018b; Thum et al. 2018). The KVN observation was conducted on 2023 February 8 (UT 20:00) with two 21 m antennas (KVN Yonsei and Tamna) combined in single-dish mode. The polarization observations were conducted in position-switching mode (Kang et al. 2015) and calibrated using an unpolarized (Jupiter) calibrator and a polarized (3C286, Agudo et al. 2012) calibrator for the polarization degree, and the Crab nebula for the polarization angle (152°; Aumont et al. 2010). The SMA observations were performed within the framework of the SMA Monitoring of AGNs with Polarization (SMAPOL) program (Ho et al. 2004; Marrone & Rao 2008; Primiani et al. 2016). The radio observations covered the frequency range from 4.85 to 225.5 GHz. At the lowest radio frequency (4.85 GHz), the polarization degree was $\Pi_{4.85\ GHz} = 2.6\% \pm 0.7\%$ along a polarization angle $\psi_{4.85\ GHz} = 133° \pm 7°$. At intermediate frequencies (22 and 43 GHz), the polarization degree was $\Pi_{22-43\ GHz} = 1\%$–2%, with $\psi_{22-43\ GHz} = 65°$–$80°$. At the higher frequencies (86 and 225 GHz), we measured $\Pi_{86-225\ GHz} \sim 3\%$ along $\psi_{86-225\ GHz} = 100°$–$120°$. We did not observe strong variability in either the degree or angle of polarization at any of the radio frequencies before, during, or after the IXPE observations (Figure 3).

Optical observations were obtained at the Calar Alto Observatory, Nordic Optical Telescope, Perkins Telescope, and Sierra Nevada Observatory. At Calar Alto Observatory, we used the 2.2 m telescope and Calar Alto Faint Object Spectrograph (CAFOS). Observations at the Sierra Nevada Observatory used the T90 telescope. The data for both observatories were taken in R band and analyzed following standard polarimetric procedures. B-, V-, R-, and I-band polarimetric observations were obtained with the Alhambra Faint Object Spectrograph and Camera (ALFOSC) at the Nordic Optical Telescope, and analyzed using Tuorla Observatory's semiautomatic data reduction pipeline (Hovatta et al. 2016; Nilsson et al. 2018). Additional photometric (B, V, R,

[69] https://fermi.gsfc.nasa.gov/ssc/data/access/lat/LightCurveRepository/
[70] http://polami.iaa.es/

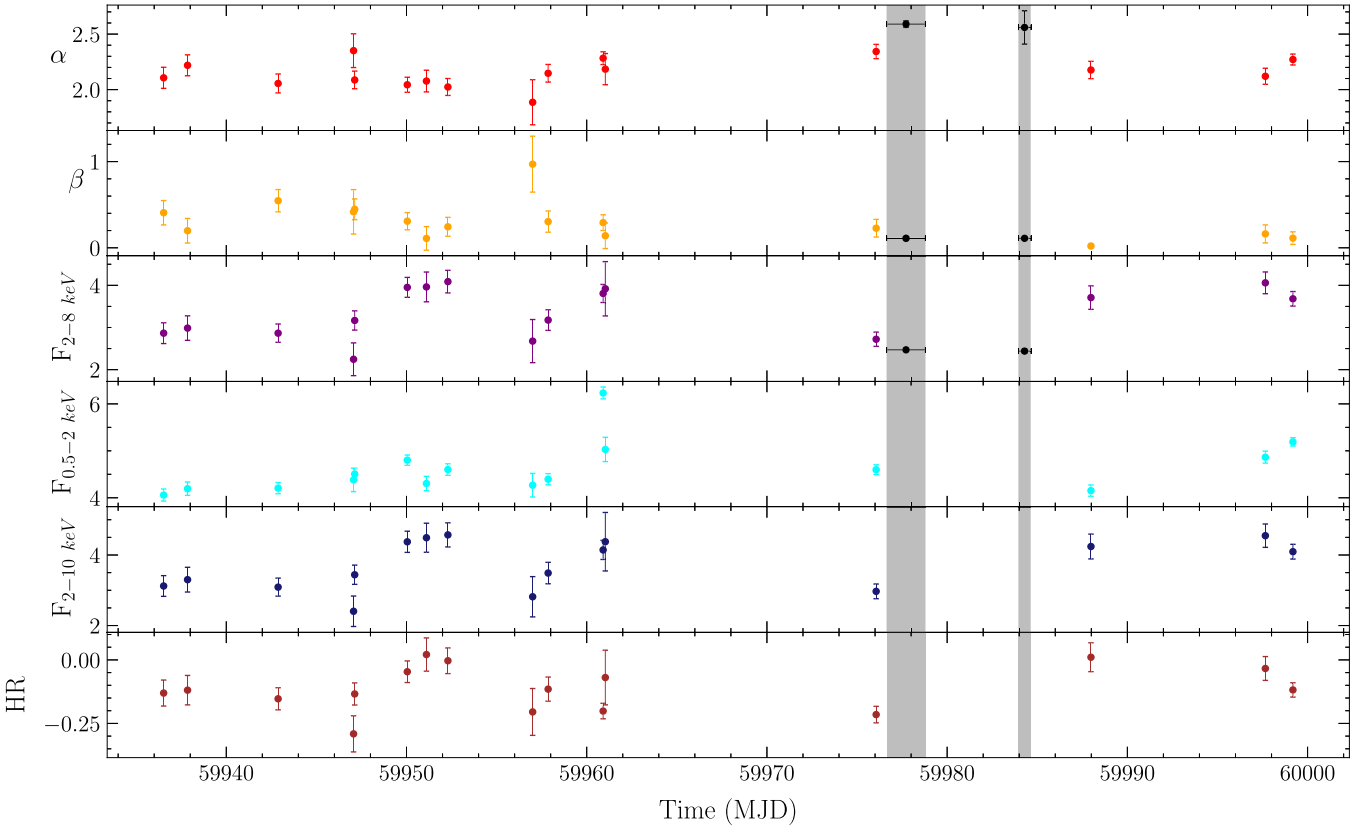

Figure 2. Results of the Swift/XRT monitoring campaign of PG 1553+113. Fluxes $F_{\rm IXPE}$, $F_{\rm Soft}$, and $F_{\rm Hard}$ are computed in the 2–8, 0.5–2, and 2–10 keV bands, respectively, and are displayed in units of 10^{-11} erg cm^{-2} s^{-1}. "HR" is the hardness ratio, defined as $(F_{\rm Hard}-F_{\rm Soft})/(F_{\rm Hard}+F_{\rm Soft})$. Gray shaded areas mark the durations of the two IXPE observations, intervals a (left) and b (right). Black data points account for the different quantities measured by IXPE and quoted in Table 2.

and *I*) and polarimetric (*R*-band) data were obtained at the Perkins Telescope (1.8 m) using the PRISM camera. During IXPE interval a, we found $\Pi_{\rm O}=2.2\%\pm0.4\%$. During interval b, we observed an increase of the polarization degree to $\Pi_{\rm O}=4.2\%\pm0.5\%$. At the same time, we observed a rotation of the polarization angle of about $\Delta\psi_R\approx125^\circ$ at a rate of about 17° day^{-1} (see Figure 3, panel (c)). The duration, amplitude, and rotation rate are within the typical rotation parameters of other blazars (e.g., Blinov et al. 2018). Compared to the two previous rotations of the optical polarization vector of PG 1553+113 detected by the RoboPol program (Blinov et al. 2015, 2016b, 2018), the event reported here has a similar amplitude, but a factor of 2–3 higher rotation rate. However, we note that, while the end of the rotation is apparent in our data, the rotation may have started before the beginning of our observations. It is therefore possible that we are underestimating the total amplitude and duration of the event.

5. Discussion and Conclusions

We have reported the first IXPE observations of the HSP blazar PG 1553+113, finding an X-ray polarization degree $\Pi_{\rm X}=(10.1\pm2.3)\%$ along an electric-vector position angle of $\psi_{\rm X}=86^\circ\pm8^\circ$. These values were obtained by performing a spectropolarimetric analysis, using XSPEC, of the *I*, *Q*, and *U* Stokes spectra that were fit with a quasi-simultaneous XMM-Newton spectrum. The source spectrum can be fit with a log-parabola, which models the curved X-ray spectrum typical of synchrotron-dominated HSP blazars (e.g., Massaro et al. 2004; Giommi et al. 2021; Middei et al. 2022).

Our contemporaneous radio and optical polarization observations find a 2.5–5 times lower polarization degree, with a polarization angle roughly aligned with the X-ray value. Previous IXPE results for the HSP blazars Mrk 421 and Mrk 501 (Di Gesu et al. 2022; Liodakis et al. 2022) have found similar chromatic behavior of Π, usually with similar ψ across different frequencies. The ratio $\Pi_{\rm X}/\Pi_{\rm O}$ is also similar to that found in Mrk 421 and Mrk 501. These results have been interpreted as evidence of an electron population that is accelerated in a shock and becomes energy stratified as it cools while propagating away from the shock front (see details in, e.g., Marscher & Gear 1985; Perlman et al. 1999; Perlman & Wilson 2005; Angelakis et al. 2016; Tavecchio et al. 2018). Given the different synchrotron cooling lengths, the optical and radio emitting particles occupy an increasing volume of the jet with decreasing frequency. In this case, the radio, optical, and X-ray emission regions are expected to be at most partially cospatial, which leads to different polarization properties in the different bands.

Rotations with time of the optical polarization angle have now been observed in a large number of blazars (e.g., Marscher et al. 2008, 2010; Blinov et al. 2016a, 2018; Liodakis et al. 2020). Recently, rotation of the X-ray polarization vector was observed for the first time, in Mrk 421 (Di Gesu et al. 2023). During this event, Mrk 421 was observed to have a variable X-ray spectral shape and flux, but no evidence was found for a change in ψ at either radio or optical wavelengths. The X-ray rotation was interpreted as a shock propagating along a helical magnetic field.

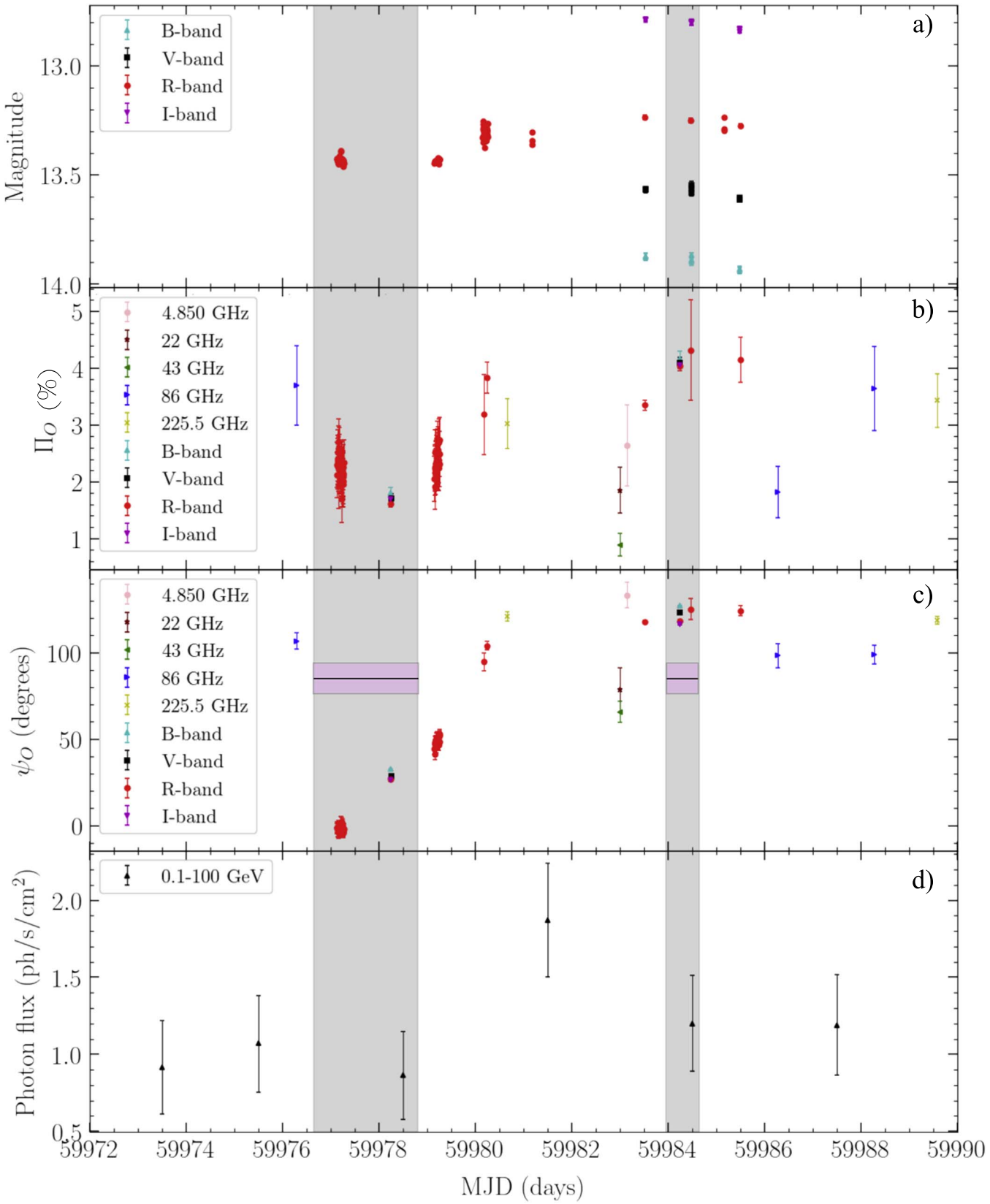

Figure 3. Multiwavelength radio and optical observations of PG 1553+113. Panel (a) shows the brightness in magnitudes, panel (b) the polarization degree, panel (c) the polarization angle, and panel (d) the γ-ray light curve in the 0.1–100 GeV range. The gray shaded areas mark the two intervals of IXPE observations. The error bars represent 1σ uncertainties. Pink boxes identify the ψ_X best-fit value and its 1σ uncertainty as derived using IXPE. Panel (d) displays the photon flux observed by the Fermi Area Telescope during the IXPE monitoring of the source. The photon flux is in units of 10^{-7} photons s^{-1} cm^{-2} (see Abdollahi et al. 2023, for details of the Fermi light curve).

In the case of PG 1553+113, we instead have observed $\Delta\psi \approx 125^\circ$ at optical wavelengths, which occurred between IXPE intervals a and b. This rotation of the optical polarization angle was accompanied by a modestly variable X-ray flux and roughly constant spectral shape. Moreover, we have found no evidence for a change in ψ in either the radio or X-ray bands. This is consistent with the interpretation of the Mrk 421 results, where the X-ray–optical–radio emission of blazars originates not from a single localized region, but rather from separate (or at most partially cospatial) regions in the jet. Moreover, as imaged with the MOJAVE program,[71] PG1553+113 is a very core-dominated source at 15 GHz, with faint extended structure at a projected position angle between 30° and 50°. This implies that the observed X-ray polarization position angle is oblique to the parsec-scale jet direction, with a difference ∼45°, similar to that observed for Mrk 421 during its first IXPE observation in 2022 May (Di Gesu et al. 2023). However, we note that the position angle of the jet is known to vary over time (Lico et al. 2020).

The origin of the optical rotation is unclear. Figure 3 (bottom panel) shows the 3 day binned γ-ray light curve of PG 1553 +113 during the IXPE observations. There is a clear brightening of the γ-rays near the center of the optical polarization angle rotation. A statistical association between optical rotations and γ-ray activity has already been established by the RoboPol program (Blinov et al. 2015, 2018), suggesting that such rotations are often deterministic rather than a random walk of the polarization angle. However, the statistics do not exclude the possibility that some rotations are indeed random walks. Kink-driven magnetic reconnection (Bodo et al. 2021) can cause variations of the polarization angle that would be different in optical and X-rays. However, in this scenario, the optically emitting particles do not travel far from the current sheet, therefore we expect a similar polarization degree in optical and X-rays (Bodo et al. 2021). The observed chromatic behavior of Π disfavors this interpretation. Merging of reconnection plasmoids can also produce orphan optical polarization rotations accompanied by multiwavelength flares (Hosking & Sironi 2020). However, the timescales of such rotations are expected to be much shorter than the ∼7 days observed here. In addition, we did not observe the expected optical flare, which makes this interpretation unlikely.

We conclude that the lower degree of polarization at optical wavelengths is most likely connected with stronger turbulence in the optical emission region. In this case, the detected rotation could have been caused by turbulence, as observed in simulated polarization angle behavior in the Turbulent Extreme MultiZone (TEMZ) model and particle-in-cell simulations (Marscher et al. 2017; Marscher & Jorstad 2021; Zhang et al. 2023).

Given the above assessment, our results favor a model where an energy-stratified—and most likely shock-accelerated—electron population is responsible for the nonthermal X-ray–optical–radio emission of at least some, and possibly all, astrophysical jets associated with SMBHs.

Acknowledgments

The Imaging X-ray Polarimetry Explorer (IXPE) is a joint US and Italian mission. The US contribution is supported by the National Aeronautics and Space Administration (NASA) and led and managed by its Marshall Space Flight Center (MSFC), with industry partner Ball Aerospace (contract NNM15AA18C). The Italian contribution is supported by the Italian Space Agency (Agenzia Spaziale Italiana, ASI) through contract ASI-OHBI-2017-12-I.0, with agreements ASI-INAF-2022-14-HH.0 and ASI-INFN 2021-43-HH.0, and its Space Science Data Center (SSDC), and by the Istituto Nazionale di Astrofisica (INAF) and the Istituto Nazionale di Fisica Nucleare (INFN) in Italy. This research used data products provided by the IXPE Team (MSFC, SSDC, INAF, and INFN) and distributed with additional software tools by the High-Energy Astrophysics Science Archive Research Center (HEASARC), at the NASA Goddard Space Flight Center (GSFC). We acknowledge financial support from ASI-INAF agreement n. 2022-14-HH.0. The research at Boston University was supported in part by National Science Foundation grant AST-2108622, NASA Fermi Guest Investigator grants 80NSSC21K1917 and 80NSSC22K1571, and NASA Swift Guest Investigator grant 80NSSC22K1482. This work was supported in part by NSF grant AST-2109127. This study was based in part on observations conducted using the Perkins Telescope Observatory (PTO) in Arizona, USA, which is owned and operated by Boston University. We acknowledge the use of public data from the Swift data archive. Based on observations obtained with XMM-Newton, an ESA science mission with instruments and contributions directly funded by ESA Member States and NASA. We acknowledge funding to support our NOT observations from the Finnish Centre for Astronomy with ESO (FINCA), University of Turku, Finland (Academy of Finland grant nr 306531). The IAA-CSIC coauthors acknowledge financial support from the Spanish "Ministerio de Ciencia e Innovación" (MCIN/AEI/ 10.13039/501100011033) through the Center of Excellence Severo Ochoa award for the Instituto de Astrofísica de Andalucía-CSIC (CEX2021-001131-S), and through grants PID2019-107847RB-C44 and PID2022-139117NB-C44. The POLAMI observations were carried out at the IRAM 30 m telescope. IRAM is supported by INSU/CNRS (France), MPG (Germany) and IGN (Spain). Part of the French contribution is supported by the Scientific Research National Center (CNRS) and the French Space Agency (CNES). Some of the data are based on observations collected at the Observatorio de Sierra Nevada, owned and operated by the Instituto de Astrofísica de Andalucía (IAA-CSIC). Further data are based on observations collected at the Centro Astronómico Hispano-Alemán (CAHA), operated jointly by Junta de Andalucía and Consejo Superior de Investigaciones Científicas (IAA-CSIC). C.C. acknowledges support by the European Research Council (ERC) under the HORIZON ERC Grants 2021 program under grant agreement No. 101040021. The Submillimetre Array is a joint project between the Smithsonian Astrophysical Observatory and the Academia Sinica Institute of Astronomy and Astrophysics and is funded by the Smithsonian Institution and the Academia Sinica. Maunakea, the location of the SMA, is a culturally important site for the indigenous Hawaiian people; we are privileged to study the cosmos from its summit. Some of the data reported here are based on observations made with the Nordic Optical Telescope, owned in collaboration with the University of Turku and Aarhus University, and operated jointly by Aarhus University, the University of Turku, and the University of Oslo, representing Denmark, Finland, and Norway, the University of Iceland, and Stockholm University

[71] https://www.cv.nrao.edu/MOJAVE/sourcepages/1553+113.shtml

at the Observatorio del Roque de los Muchachos, La Palma, Spain, of the Instituto de Astrofisica de Canarias. E.L. was supported by Academy of Finland projects 317636 and 320045. The data presented here were obtained in part with ALFOSC, which is provided by the Instituto de Astrofisica de Andalucia (IAA) under a joint agreement with the University of Copenhagen and NOT. S.K., S.-S.L., W.Y.C., S.-H.K., and H.-W.J. were supported by the National Research Foundation of Korea (NRF) grant funded by the Korea government (MIST; 2020R1A2C2009003). The KVN is a facility operated by the Korea Astronomy and Space Science Institute. The KVN operations are supported by KREONET (Korea Research Environment Open NETwork), which is managed and operated by KISTI (Korea Institute of Science and Technology Information). Partly based on observations with the 100 m telescope of the MPIfR (Max-Planck-Institut für Radioastronomie) at Effelsberg. Observations with the 100 m radio telescope at Effelsberg have received funding from the European Union's Horizon 2020 research and innovation program under grant agreement No 101004719 (ORP).

Facilities: CAO:2.2m, Effelsberg, Fermi, IRAM 30 m, IXPE, KVN, NOT, Perkins, SMA, Swift, OSN:0.9m, and XMM.

ORCID iDs

Riccardo Middei https://orcid.org/0000-0001-9815-9092
Matteo Perri https://orcid.org/0000-0003-3613-4409
Ioannis Liodakis https://orcid.org/0000-0001-9200-4006
Alan P. Marscher https://orcid.org/0000-0001-7396-3332
Nicole Rodriguez Cavero https://orcid.org/0000-0001-5256-0278
Fabrizio Tavecchio https://orcid.org/0000-0003-0256-0995
Immacolata Donnarumma https://orcid.org/0000-0002-4700-4549
Marco Laurenti https://orcid.org/0000-0001-5762-6360
Svetlana G. Jorstad https://orcid.org/0000-0001-6158-1708
Iván Agudo https://orcid.org/0000-0002-3777-6182
Herman L. Marshall https://orcid.org/0000-0002-6492-1293
Luigi Pacciani https://orcid.org/0000-0001-6897-5996
Dawoon E. Kim https://orcid.org/0000-0001-5717-3736
Giacomo Bonnoli https://orcid.org/0000-0003-2464-9077
Beatriz Agís-González https://orcid.org/0000-0001-7702-8931
Carolina Casadio https://orcid.org/0000-0003-1117-2863
Juan Escudero https://orcid.org/0000-0002-4131-655X
Ioannis Myserlis https://orcid.org/0000-0003-3025-9497
Pouya M. Kouch https://orcid.org/0000-0002-9328-2750
Mark Gurwell https://orcid.org/0000-0003-0685-3621
Garrett K. Keating https://orcid.org/0000-0002-3490-146X
Sincheol Kang https://orcid.org/0000-0002-0112-4836
Sang-Sung Lee https://orcid.org/0000-0002-6269-594X
Sang-Hyun Kim https://orcid.org/0000-0001-7556-8504
Whee Yeon Cheong https://orcid.org/0009-0002-1871-5824
Hyeon-Woo Jeong https://orcid.org/0009-0005-7629-8450
Alexander Kraus https://orcid.org/0000-0002-4184-9372
Lucio A. Antonelli https://orcid.org/0000-0002-5037-9034
Matteo Bachetti https://orcid.org/0000-0002-4576-9337
Luca Baldini https://orcid.org/0000-0002-9785-7726
Wayne H. Baumgartner https://orcid.org/0000-0002-5106-0463
Ronaldo Bellazzini https://orcid.org/0000-0002-2469-7063
Stefano Bianchi https://orcid.org/0000-0002-4622-4240
Stephen D. Bongiorno https://orcid.org/0000-0002-0901-2097
Raffaella Bonino https://orcid.org/0000-0002-4264-1215
Alessandro Brez https://orcid.org/0000-0002-9460-1821
Niccolò Bucciantini https://orcid.org/0000-0002-8848-1392
Fiamma Capitanio https://orcid.org/0000-0002-6384-3027
Simone Castellano https://orcid.org/0000-0003-1111-4292
Elisabetta Cavazzuti https://orcid.org/0000-0001-7150-9638
Chien-Ting Chen https://orcid.org/0000-0002-4945-5079
Stefano Ciprini https://orcid.org/0000-0002-0712-2479
Enrico Costa https://orcid.org/0000-0003-4925-8523
Alessandra De Rosa https://orcid.org/0000-0001-5668-6863
Ettore Del Monte https://orcid.org/0000-0002-3013-6334
Niccolò Di Lalla https://orcid.org/0000-0002-7574-1298
Alessandro Di Marco https://orcid.org/0000-0003-0331-3259
Victor Doroshenko https://orcid.org/0000-0001-8162-1105
Michal Dovčiak https://orcid.org/0000-0003-0079-1239
Steven R. Ehlert https://orcid.org/0000-0003-4420-2838
Teruaki Enoto https://orcid.org/0000-0003-1244-3100
Yuri Evangelista https://orcid.org/0000-0001-6096-6710
Sergio Fabiani https://orcid.org/0000-0003-1533-0283
Riccardo Ferrazzoli https://orcid.org/0000-0003-1074-8605
Javier A. García https://orcid.org/0000-0003-3828-2448
Shuichi Gunji https://orcid.org/0000-0002-5881-2445
Jeremy Heyl https://orcid.org/0000-0001-9739-367X
Wataru Iwakiri https://orcid.org/0000-0002-0207-9010
Philip Kaaret https://orcid.org/0000-0002-3638-0637
Vladimir Karas https://orcid.org/0000-0002-5760-0459
Fabian Kislat https://orcid.org/0000-0001-7477-0380
Jeffery J. Kolodziejczak https://orcid.org/0000-0002-0110-6136
Henric Krawczynski https://orcid.org/0000-0002-1084-6507
Fabio La Monaca https://orcid.org/0000-0001-8916-4156
Luca Latronico https://orcid.org/0000-0002-0984-1856
Simone Maldera https://orcid.org/0000-0002-0698-4421
Alberto Manfreda https://orcid.org/0000-0002-0998-4953
Frédéric Marin https://orcid.org/0000-0003-4952-0835
Andrea Marinucci https://orcid.org/0000-0002-2055-4946
Francesco Massaro https://orcid.org/0000-0002-1704-9850
Giorgio Matt https://orcid.org/0000-0002-2152-0916
Tsunefumi Mizuno https://orcid.org/0000-0001-7263-0296
Fabio Muleri https://orcid.org/0000-0003-3331-3794
Michela Negro https://orcid.org/0000-0002-6548-5622
Chi-Yung Ng https://orcid.org/0000-0002-5847-2612
Stephen L. O'Dell https://orcid.org/0000-0002-1868-8056
Nicola Omodei https://orcid.org/0000-0002-5448-7577
Chiara Oppedisano https://orcid.org/0000-0001-6194-4601
Alessandro Papitto https://orcid.org/0000-0001-6289-7413
George G. Pavlov https://orcid.org/0000-0002-7481-5259
Abel L. Peirson https://orcid.org/0000-0001-6292-1911
Melissa Pesce-Rollins https://orcid.org/0000-0003-1790-8018
Pierre-Olivier Petrucci https://orcid.org/0000-0001-6061-3480
Maura Pilia https://orcid.org/0000-0001-7397-8091
Andrea Possenti https://orcid.org/0000-0001-5902-3731

Juri Poutanen https://orcid.org/0000-0002-0983-0049
Brian D. Ramsey https://orcid.org/0000-0003-1548-1524
John Rankin https://orcid.org/0000-0002-9774-0560
Ajay Ratheesh https://orcid.org/0000-0003-0411-4243
Oliver J. Roberts https://orcid.org/0000-0002-7150-9061
Roger W. Romani https://orcid.org/0000-0001-6711-3286
Carmelo Sgrò https://orcid.org/0000-0001-5676-6214
Patrick Slane https://orcid.org/0000-0002-6986-6756
Paolo Soffitta https://orcid.org/0000-0002-7781-4104
Gloria Spandre https://orcid.org/0000-0003-0802-3453
Douglas A. Swartz https://orcid.org/0000-0002-2954-4461
Toru Tamagawa https://orcid.org/0000-0002-8801-6263
Roberto Taverna https://orcid.org/0000-0002-1768-618X
Allyn F. Tennant https://orcid.org/0000-0002-9443-6774
Nicholas E. Thomas https://orcid.org/0000-0003-0411-4606
Francesco Tombesi https://orcid.org/0000-0002-6562-8654
Alessio Trois https://orcid.org/0000-0002-3180-6002
Sergey S. Tsygankov https://orcid.org/0000-0002-9679-0793
Roberto Turolla https://orcid.org/0000-0003-3977-8760
Jacco Vink https://orcid.org/0000-0002-4708-4219
Martin C. Weisskopf https://orcid.org/0000-0002-5270-4240
Kinwah Wu https://orcid.org/0000-0002-7568-8765
Fei Xie https://orcid.org/0000-0002-0105-5826
Silvia Zane https://orcid.org/0000-0001-5326-880X

References

Abdo, A. A., Ackermann, M., Agudo, I., et al. 2010, ApJ, 716, 30
Abdollahi, S., Ajello, M., Baldini, L., et al. 2023, ApJS, 265, 31
Acero, F., Ackermann, M., Ajello, M., et al. 2015, ApJS, 218, 23
Ackermann, M., Ajello, M., Albert, A., et al. 2015, ApJL, 813, L41
Agudo, I., Jorstad, S. G., Marscher, A. P., et al. 2011a, ApJL, 726, L13
Agudo, I., Marscher, A. P., Jorstad, S. G., et al. 2011b, ApJL, 735, L10
Agudo, I., Thum, C., Molina, S. N., et al. 2018a, MNRAS, 474, 1427
Agudo, I., Thum, C., Ramakrishnan, V., et al. 2018b, MNRAS, 473, 1850
Agudo, I., Thum, C., Wiesemeyer, H., et al. 2012, A&A, 541, A111
Ajello, M., Angioni, R., Axelsson, M., et al. 2020, ApJ, 892, 105
Aleksić, J., Alvarez, E. A., Antonelli, L. A., et al. 2012, ApJ, 748, 46
Angel, J. R. P., & Stockman, H. S. 1980, ARA&A, 18, 321
Angelakis, E., Hovatta, T., Blinov, D., et al. 2016, MNRAS, 463, 3365
Antonucci, R. 1993, ARA&A, 31, 473
Arnaud, K. A. 1996, in ASP Conf. Ser. 101, Astronomical Data Analysis Software and Systems V, ed. G. H. Jacoby & J. Barnes (San Francisco, CA: ASP), 17
Aumont, J., Conversi, L., Thum, C., et al. 2010, A&A, 514, A70
Baldini, L., Barbanera, M., Bellazzini, R., et al. 2021, APh, 133, 102628
Baldini, L., Bucciantini, N., Lalla, N. D., et al. 2022, SoftX, 19, 101194
Bellazzini, R., Angelini, F., Baldini, L., et al. 2003, Proc. SPIE, 4843, 383
Blandford, R., Meier, D., & Readhead, A. 2019, ARA&A, 57, 467
Blinov, D., Pavlidou, V., Papadakis, I., et al. 2015, MNRAS, 453, 1669
Blinov, D., Pavlidou, V., Papadakis, I., et al. 2016a, MNRAS, 462, 1775
Blinov, D., Pavlidou, V., Papadakis, I., et al. 2018, MNRAS, 474, 1296
Blinov, D., Pavlidou, V., Papadakis, I. E., et al. 2016b, MNRAS, 457, 2252
Bodo, G., Tavecchio, F., & Sironi, L. 2021, MNRAS, 501, 2836
Boettcher, M. 2012, arXiv:1205.0539
Cerruti, M., Zech, A., Boisson, C., & Inoue, S. 2015, MNRAS, 448, 910
Costa, E., Soffitta, P., Bellazzini, R., et al. 2001, Natur, 411, 662
Di Gesu, L., Donnarumma, I., Tavecchio, F., et al. 2022, ApJL, 938, L7
Di Gesu, L., Marshall, H. L., Ehlert, S. R., et al. 2023, NatAs, Advanced Online Publication
Di Marco, A., Costa, E., Muleri, F., et al. 2022, AJ, 163, 170
Di Marco, A., Soffitta, P., Costa, E., et al. 2023, AJ, 165, 143
Dorigo Jones, J., Johnson, S. D., Muzahid, S., et al. 2022, MNRAS, 509, 4330
Ehlert, S. R., Ferrazzoli, R., Marinucci, A., et al. 2022, ApJ, 935, 116
Fossati, G., Maraschi, L., Celotti, A., Comastri, A., & Ghisellini, G. 1998, MNRAS, 299, 433
Gabriel, C., Denby, M., Fyfe, D. J., et al. 2004, in ASP Conf. Ser. 314, Astronomical Data Analysis Software and Systems (ADASS) XIII, ed. F. Ochsenbein, M. G. Allen, & D. Egret (San Francisco, CA: ASP), 759
Gehrels, N., Chincarini, G., Giommi, P., et al. 2004, ApJ, 611, 38
Ghisellini, G., Celotti, A., Fossati, G., Maraschi, L., & Comastri, A. 1998, MNRAS, 301, 451
Gianolli, V. E., Kim, D. E., Bianchi, S., et al. 2023, MNRAS, 523, 4468
Giommi, P., Perri, M., Capalbi, M., et al. 2021, MNRAS, 507, 5690
HI4PI Collaboration, Ben Bekhti, N., Flöer, L., et al. 2016, A&A, 594, A116
Ho, P. T. P., Moran, J. M., & Lo, K. Y. 2004, ApJL, 616, L1
Hosking, D. N., & Sironi, L. 2020, ApJL, 900, L23
Hovatta, T., & Lindfors, E. 2019, NewAR, 87, 101541
Hovatta, T., Lindfors, E., Blinov, D., et al. 2016, A&A, 596, A78
Hovatta, T., Valtaoja, E., Tornikoski, M., & Lähteenmäki, A. 2009, A&A, 494, 527
Ingram, A., Ewing, M., Marinucci, A., et al. 2023, arXiv:2305.13028
Jansen, F., Lumb, D., Altieri, B., et al. 2001, A&A, 365, L1
Jethwa, P., Saxton, R., Guainazzi, M., Rodriguez-Pascual, P., & Stuhlinger, M. 2015, A&A, 581, A104
Johnson, S. D., Mulchaey, J. S., Chen, H.-W., et al. 2019, ApJL, 884, L31
Kang, S., Lee, S.-S., & Byun, D.-Y. 2015, JKAS, 48, 257
Kraus, A., Krichbaum, T. P., Wegner, R., et al. 2003, A&A, 401, 161
Lähteenmäki, A., & Valtaoja, E. 1999, ApJ, 521, 493
Lico, R., Liu, J., Giroletti, M., et al. 2020, A&A, 634, A87
Liodakis, I., Blinov, D., Jorstad, S. G., et al. 2020, ApJ, 902, 61
Liodakis, I., Hovatta, T., Huppenkothen, D., et al. 2018a, ApJ, 866, 137
Liodakis, I., Marscher, A. P., Agudo, I., et al. 2022, Natur, 611, 677
Liodakis, I., Romani, R. W., Filippenko, A. V., et al. 2018b, MNRAS, 480, 5517
Liodakis, I., Romani, R. W., Filippenko, A. V., Kocevski, D., & Zheng, W. 2019, ApJ, 880, 32
Maraschi, L., Ghisellini, G., & Celotti, A. 1992, ApJL, 397, L5
Marinucci, A., Muleri, F., Dovciak, M., et al. 2022, MNRAS, 516, 5907
Marrone, D. P., & Rao, R. 2008, Proc. SPIE, 7020, 70202B
Marscher, A., Jorstad, S., & Williamson, K. 2017, Galax, 5, 63
Marscher, A. P., & Gear, W. K. 1985, ApJ, 298, 114
Marscher, A. P., & Jorstad, S. G. 2021, Galax, 9, 27
Marscher, A. P., Jorstad, S. G., D'Arcangelo, F. D., et al. 2008, Natur, 452, 966
Marscher, A. P., Jorstad, S. G., Larionov, V. M., et al. 2010, ApJL, 710, L126
Maselli, A., Massaro, E., Nesci, R., et al. 2010, A&A, 512, A74
Massaro, E., Perri, M., Giommi, P., & Nesci, R. 2004, A&A, 413, 489
Middei, R., Giommi, P., Perri, M., et al. 2022, MNRAS, 514, 3179
Middei, R., Liodakis, I., Perri, M., et al. 2023, ApJL, 942, L10
Myserlis, I., Angelakis, E., Kraus, A., et al. 2018, A&A, 609, A68
Nicastro, F., Kaastra, J., Krongold, Y., et al. 2018, Natur, 558, 406
Nilsson, K., Lindfors, E., Takalo, L. O., et al. 2018, A&A, 620, A185
Padovani, P., Alexander, D. M., Assef, R. J., et al. 2017, A&ARv, 25, 2
Padovani, P., & Giommi, P. 1995, ApJ, 444, 567
Peirson, A. L., Negro, M., Liodakis, I., et al. 2023, ApJL, 948, L25
Perlman, E. S., Biretta, J. A., Zhou, F., Sparks, W. B., & Macchetto, F. D. 1999, AJ, 117, 2185
Perlman, E. S., & Wilson, A. S. 2005, ApJ, 627, 140
Pesce-Rollins, M., Lalla, N. D., Omodei, N., & Baldini, L. 2019, NIMPA, 936, 224
Piconcelli, E., Jimenez-Bailón, E., Guainazzi, M., et al. 2004, MNRAS, 351, 161
Primiani, R. A., Young, K. H., Young, A., et al. 2016, JAI, 5, 1641006
Sreekumar, P., Bertsch, D. L., Dingus, B. L., et al. 1998, ApJ, 494, 523
Strüder, L., Briel, U., Dennerl, K., et al. 2001, A&A, 365, L18
Tagliacozzo, D., Marinucci, A., Ursini, F., et al. 2023, arXiv:2305.10213
Tavani, M., Cavaliere, A., Munar-Adrover, P., & Argan, A. 2018, ApJ, 854, 11
Tavecchio, F., Landoni, M., Sironi, L., & Coppi, P. 2018, MNRAS, 480, 2872
Thum, C., Agudo, I., Molina, S. N., et al. 2018, MNRAS, 473, 2506
Urry, C. M., & Padovani, P. 1995, PASP, 107, 803
Ursini, F., Marinucci, A., Matt, G., et al. 2023, MNRAS, 519, 50
Weisskopf, M. C., Soffitta, P., Baldini, L., et al. 2022, JATIS, 8, 026002
Zhang, H., Marscher, A. P., Guo, F., et al. 2023, ApJ, 949, 71